Performance of an Array of Circular Waveguides with Strip-Loaded Dielectric Hard Walls

Sergei P. Skobelev, *Member, IEEE,* and Per-Simon Kildal, *Fellow, IEEE*

***Abstract*—An infinite planar periodic antenna array of radiating open-ended circular waveguides is considered. The conducting waveguide walls are covered with dielectric layers loaded with longitudinal conducting strips for providing the hard wall boundary condition. Analysis of the array is carried out by the mode-matching method. The waveguide modes involved in the method are calculated by using the asymptotic strip boundary condition. It is shown that they are split into an independent subsystem of TE modes for the whole cross section and two independent subsystems of TM modes: one is for the central region and another is for the layer region. The calculations show that the operation of the hard waveguides in an array with small element spacing is similar to that of the multimode smooth wall waveguides completely filled with dielectric. For large diameters and element spacing, the hard waveguides have significant advantages over the smooth ones. It is shown that unlike an individual hard waveguide, the aperture efficiency of such a waveguide in array has a nonmonotonic dependence on the waveguide radius. The results characterizing the behavior of the aperture efficiency and cross-polarization level in a frequency band as well as the contribution of certain waveguide modes in the reflected power are presented and discussed. The examples of the element patterns corresponding to minimal cross polarization are also given.**

***Index Terms*—Antenna arrays, waveguides.**

I. Introduction

AN ATTRACTIVE modern horn antenna is a conical horn in which the inner metallic surface is coated with a dielectric layer, which is loaded with longitudinal conducting strips to provide the so-called hard wall boundary condition [1]. Such a horn is easy to fabricate and it can potentially provide both high-aperture efficiency and low cross polarization due to the presence of a uniform copolar field distribution over the central part of its aperture at the design frequency. A good model of such a hard wall horn, when the flare angle is small, is the corresponding open-ended waveguide. Such a hard strip-loaded circular waveguide model has been studied in [2] and [3], where there have been presented calculated characteristics of the operating modified TE_{11} mode and stripline mode for the first (dominant) azimuth harmonic as well as the corresponding radiation patterns, aperture efficiency, and cross polarization obtained by the Huygen–Kirchoff integration method. The presented results show good capabilities of the hard strip-loaded horn as an individual antenna and, in this connection, it is of interest to study the performance of such a horn as an element of an array. In this case, however, the electromagnetic interaction always existing between the array elements leads to excitation of not only the dominant mode at the horn aperture but also the modes of other orders and all these modes should be taken into account in the array analysis.

In the present paper, the performance of the hard strip-loaded circular horn in an array is studied on the basis of solving a problem about radiation from an infinite planar periodic antenna array of the corresponding open-ended waveguides. The problem is solved by the mode-matching method [4], which implies involving a complete system of vector Floquet harmonics in free-space and a complete system of vector harmonics in the waveguide. Unlike the Floquet harmonics, which are well known [5], the hard strip-loaded waveguide harmonics have not been considered in the literature except for the particular case in papers [2] and [3] mentioned above. The calculation of the propagation constants and construction of the system of waveguide harmonics is carried out below on the basis of using the asymptotic strip boundary condition [6], according to which the strips are replaced by a continuous anisotropically conducting tube. Such a replacement considerably simplifies the calculations in comparison with those made in [3] on the basis of the integral equation method and at the same time, as shown for other similar problems, it gives good agreement both with experimental data and with the results obtained by much more complex methods [7], [8].

II. Formulation and Solution of the Problem

A. Geometry and Excitation of the Array

Consider an infinite planar array of semi-infinite open-ended circular waveguides arranged in a regular rectangular or triangular lattice in the plane $0xy$ of a Cartesian rectangular coordinate system $0xyz$ with the corresponding unit vectors $\boldsymbol{e}_x$, $\boldsymbol{e}_y$, and $\boldsymbol{e}_z$, as shown in Fig. 1(a) where d_x is the element spacing in a row, d_y is the spacing between the rows, and Δ is a shift of the neighbor rows with respect to each other equal to $d_x/2$ for a triangular lattice or zero for a rectangular one. All the waveguide openings have a common flange, and the waveguide walls of radius b are coated with dielectric layers of relative permittivity ε and thickness $t = b - a$, where a is the radius of the empty central part [Fig. 1(b)]. The inner surfaces of the layers are loaded with longitudinal metal strips of zero thickness. The flange, waveguide walls, and strips are assumed to be perfectly conducting and the strip width and spacing are much smaller than the operating wavelength λ, so that we can approximately

Manuscript received October 6, 1999; revised January 31, 2000. This work was supported by Chalmers University of Technology, Gothenburg, Sweden, under Contract 643/16787918/00015.

S. P. Skobelev is with JSC "Radiophyszika," Moscow 123363, Russia.

P.-S. Kildal is with the Department of Electromagnetics, Chalmers University of Technology, S-412 96 Gothenburg, Sweden.

Publisher Item Identifier S 0018-926X(00)06934-9.

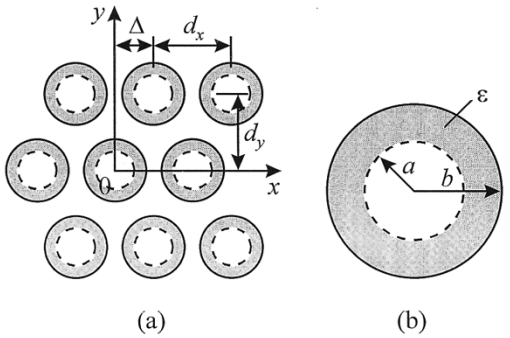

Fig. 1. (a) Geometry of array face. (b) Cross section of waveguide.

replace the strips by an anisotropic tube perfectly conducting in the longitudinal direction only.

Let the waveguides be excited by the operating modes to be determined below, propagating toward the apertures as well as having identical amplitudes and linearly progressing phases in x- and y-directions specifying the direction of the main beam. Under these conditions, it is required to determine the radiated and reflected fields and, on the basis of them, to calculate the array characteristics.

B. Modes in the Hard Strip-Loaded Waveguide

The problem formulated above will be solved by the mode-matching method that implies, in particular, involving a complete system of eigenmodes in the waveguide. To determine the waveguide modes, we will follow the general approach applied in [9] for similar problems.

Omitting the time dependence factor $\exp(-i\omega t)$, we write the electric and magnetic fields for the mth azimuth harmonics in the waveguide in the following form:

$$\begin{aligned}\boldsymbol{E} &= i\omega\mu_0 \operatorname{rot}\Pi_1 + (\operatorname{grad}\operatorname{div} + k^2\tilde{\varepsilon})\Pi_2\\ \boldsymbol{H} &= (\operatorname{grad}\operatorname{div} + k^2\tilde{\varepsilon})\Pi_1 - i\omega\varepsilon_0\tilde{\varepsilon}\operatorname{rot}\Pi_2\end{aligned} \tag{1}$$

where

$$\begin{aligned}\Pi_1(\rho, \varphi, z) &= \boldsymbol{e}_z\Phi_1(\rho)e^{i\gamma z}\cos m\varphi,\\ \Pi_2(\rho, \varphi, z) &= \boldsymbol{e}_z\Phi_2(\rho)e^{i\gamma z}\sin m\varphi\end{aligned} \tag{2}$$

are longitudinally directed magnetic and electric Hertz vectors, respectively,

$$\Phi_l(\rho) = \begin{cases} A_l J_m(g\rho), & 0 \le \rho \le a\\ B_l J_m(\hat{g}\rho) + C_l N_m(\hat{g}\rho), & a \le \rho \le b\end{cases} \tag{3}$$

A_l, B_l, and C_l, ($l = 1, 2$), are unknown amplitude constants, $J_m(\cdots)$ and $N_m(\cdots)$ are the Bessel and Neumann functions of the mth order, respectively, g and $\hat{g}$ are transverse propagation constants for the central ($\tilde{\varepsilon} = 1$) and layer ($\tilde{\varepsilon} = \varepsilon$) regions, respectively, related to the longitudinal propagation constant γ by the formula

$$\gamma^2 = k^2 - g^2 = k^2\varepsilon - \hat{g}^2 \tag{4}$$

$k = 2\pi/\lambda = \omega\sqrt{\varepsilon_0\mu_0}$ is the wavenumber, and ε_0, μ_0 are dielectric and magnetic constants of free-space. The polar coordinated ρ and φ with the corresponding unit vectors $\boldsymbol{e}_\rho$ and $\boldsymbol{e}_\varphi$ are related to the Cartesian's ones by the ordinary way: $x = \rho\cos\varphi$ and $y = \rho\sin\varphi$.

The electromagnetic field (1) must satisfy a boundary condition $\boldsymbol{e}_\rho \times \boldsymbol{E}(b, \varphi, z) = 0$ on the perfectly conducting wall, as well as a boundary condition on the inner surface of the layer loaded with strips. Assuming that the strip width and spacing (period) is small enough (smaller than 0.1λ, [7], [8]), we replace the strips by a continuous longitudinally conducting tube and apply the asymptotic strip boundary condition (ASBC) [6] to such a boundary. According to the ASBC, the longitudinal electric component must vanish on the tube, i.e., $E_z(a, \varphi, z) = 0$, while the azimuthal electric and longitudinal magnetic components must be continuous across the tube: $E_\varphi(a - 0, \varphi, z) = E_\varphi(a + 0, \varphi, z)$, $H_z(a - 0, \varphi, z) = H_z(a + 0, \varphi, z)$. Substituting (2) and (3) into (1), performing the differentiation, and satisfying the indicated boundary conditions, we obtain the following system of equations for the amplitude and propagation constants indicated above:

$$\begin{cases} B_1 J_m(\hat{g}a) + C_1 N_m(\hat{g}a) = g^2 A_1 J_m(ga)/\hat{g}^2\\ B_1 J'_m(\hat{g}a) + C_1 N'_m(\hat{g}a) = g A_1 J'_m(ga)/\hat{g}\\ B_1 J'_m(\hat{g}b) + C_1 N'_m(\hat{g}b) = 0\end{cases} \tag{5}$$

$$A_2 J_m(ga) = 0 \tag{6}$$

$$\begin{cases} B_2 J_m(\hat{g}a) + C_2 N_m(\hat{g}a) = 0\\ B_2 J_m(\hat{g}b) + C_2 N_m(\hat{g}b) = 0.\end{cases} \tag{7}$$

As we can see, the obtained system consists of an independent subsystem (5) of TE modes and two additional independent subsystems (6) and (7) of TM modes in the central and layer regions, respectively. This result, differing from the case of a waveguide loaded with a dielectric layer without strips, where only axially symmetrical TE and TM modes are decoupled while the others are not, has a simple physical interpretation. The currents of the TM modes have no transverse components and, therefore, the longitudinally conducting tube is equivalent to an ordinary isotropically conducting one. Therefore, from the viewpoint of the TM modes, the waveguide under consideration consists of two isolated regions: an empty circular waveguide of radius a and a coaxial waveguide filled with dielectric. For the TE modes, the longitudinally conducting tube is "transparent" for the tangential electric field component and, therefore, the indicated regions are not isolated.

The constants B_1 and C_1 are determined from the first two equations of (5) by the formulas

$$B_1 = \pi ga\,\frac{gJ_m(ga)N'_m(\hat{g}a) - \hat{g}J'_m(ga)N_m(\hat{g}a)}{2\hat{g}}\,A_1 \tag{8}$$

$$C_1 = -\pi ga\,\frac{gJ_m(ga)J'_m(\hat{g}a) - \hat{g}J'_m(ga)J_m(\hat{g}a)}{2\hat{g}}\,A_1. \tag{9}$$

Substitution of (8) and (9) into the third equation of (5) leads to the dispersion equation

$$\frac{1}{ga}\,\frac{J'_m(ga)}{J_m(ga)} = \frac{1}{\hat{g}a}\,\frac{J'_m(\hat{g}a)N'_m(\hat{g}b) - N'_m(\hat{g}a)J'_m(\hat{g}b)}{J_m(\hat{g}a)N'_m(\hat{g}b) - N_m(\hat{g}a)J'_m(\hat{g}b)}. \tag{10}$$

for g and $\hat{g}$, which is to be solved together with the additional relation (4).

Designating the roots of (10) as g_{1mn} and $\hat{g}_{1mn}$, $n = 1, 2, \cdots$, as well as taking into account the polarization degeneration of the axially nonsymmetrical modes, we can construct the following system of orthonormalized transverse vector wave functions for the TE modes

$$
\begin{aligned}
{}^{V}_{H}\Phi_{1mn}(\rho, \varphi) = &\pm \boldsymbol{e}_{\rho} \frac{m}{\rho} \frac{J_m(g_{1mn}\rho)}{N_{1mn}} \begin{bmatrix} \sin \\ \cos \end{bmatrix} m\varphi \\
&+ \boldsymbol{e}_{\varphi} \frac{g_{1mn} J'_m(g_{1mn}\rho)}{N_{1mn}} \begin{bmatrix} \cos \\ \sin \end{bmatrix} m\varphi \quad (11)
\end{aligned}
$$

written for the central region ($0 \le \rho \le a$) of the waveguide in the form similar to that used in [5] for the vertical (V) and horizontal (H) polarization. The corresponding expression for the layer region ($a \le \rho \le b$) is obtained from (11) by substitution of g_{1mn} and $J_m(g_{1mn}\rho)$ by $\hat{g}_{1mn}$ and $Z_{1m}(\hat{g}_{1mn}\rho) = \hat{B}_1 J_m(\hat{g}_{1mn}\rho) + \hat{C}_1 N_m(\hat{g}_{1mn}\rho)$, respectively, where $\hat{B}_1$ and $\hat{C}_1$ are determined by the coefficients in front of A_1 in (8) and (9). The normalizing coefficient N_{1mn} in (11) is determined by formula

$$
\begin{aligned}
&N_{1mn} \\
&= \left\{ (1+\delta_{0m})\pi \left[gaJ_m(ga)J'_m(ga) \right.\right. \\
&\quad + \frac{(g^2a^2 - m^2)J^2_m(ga)}{2} - \hat{g}aZ_{1m}(\hat{g}a)Z'_{1m}(\hat{g}a) \\
&\quad \left.\left. - \frac{(\hat{g}^2a^2 - m^2)Z^2_{1m}(\hat{g}a) - (\hat{g}^2b^2 - m^2)Z^2_{1m}(\hat{g}b)}{2} \right] \right\}^{1/2}
\end{aligned}
$$

where δ_{0m} is the Kronecker symbol and the subscripts at g_{1mn} and $\hat{g}_{1mn}$ are omitted for brevity.

The vector wave functions for the TM modes are available in a more general form in [5]. We write them here for the central region in the following notations:

$$
\begin{aligned}
{}^{V}_{H}\Phi_{2mn}(\rho, \varphi) = &\boldsymbol{e}_{\rho} \frac{g_{2mn} J'_m(g_{2mn}\rho)}{N_{2mn}} \begin{bmatrix} \sin \\ \cos \end{bmatrix} m\varphi \\
&\pm \boldsymbol{e}_{\varphi} \frac{m}{\rho} \frac{J_m(g_{2mn}\rho)}{N_{2mn}} \begin{bmatrix} \cos \\ \sin \end{bmatrix} m\varphi \quad (12)
\end{aligned}
$$

where $N_{2mn} = \sqrt{\pi/(2-\delta_{0m})}\, g_{2mn} a J_{m+1}(g_{2mn}a)$ are the normalizing coefficients, and g_{2mn} are roots of equation (6). The wave functions for the TM modes in the layer region ${}^{V}_{H}\hat{\Phi}_{2mn}(\rho, \varphi)$, when $m \neq 0$ and $n \neq 1$ simultaneously, are determined by an expression obtained from (12) by substitution of g_{2mn}, $J_m(g_{2mn}\rho)$, and N_{2mn} by $\hat{g}_{2mn}$, $Z_{2m}(\hat{g}_{2mn}\rho) = N_m(\hat{g}_{2mn}a)J_m(\hat{g}_{2mn}\rho) - J_m(\hat{g}_{2mn}a)N_m(\hat{g}_{2mn}\rho)$, and $\hat{N}_{2mn} = \{[2(1+\delta_{0m})/\pi][J^2_m(\hat{g}_{2mn}a)/J^2_m(\hat{g}_{2mn}b) - 1]\}^{1/2}$, respectively, where $\hat{g}_{2mn}$ are roots of the equation $N_m(\hat{g}a)J_m(\hat{g}b) - J_m(\hat{g}a)N_m(\hat{g}b) = 0$ resulted from (7). The case of $m = 0$ and $n = 1$ corresponds to the nondegenerated TEM mode for which

$$
\hat{\Phi}_{201}(\rho, \varphi) = \frac{1}{\sqrt{2\pi \ln(b/a)}} \frac{1}{\rho} \boldsymbol{e}_{\rho}. \quad (13)
$$

C. Application of the Mode-Matching Method

Having determined the system of the waveguide modes, we can now apply the mode-matching method for the further solution of the problem. Representing the total field in the waveguide as an infinite sum of incident and reflected waves, we write its transverse components in the central part of the aperture in the form

$$
\begin{aligned}
\boldsymbol{E}_{\tau}(\rho, \varphi, -0) = &\sqrt{\mu_0/\varepsilon_0} \sum_{m,n} [({}^{V}_{H}A_{1mn} + {}^{V}_{H}R_{1mn})k^{V}_{H} \\
&\cdot \Phi_{1mn}(\rho, \varphi) - {}^{V}_{H}R_{2mn}\gamma_{2mn}{}^{V}_{H}\Phi_{2mn}(\rho, \varphi)] \quad (14) \\
&- \boldsymbol{e}_z \times \boldsymbol{H}(\rho, \varphi, -0) \\
= &\sum_{m,n} [({}^{V}_{H}A_{1mn} - {}^{V}_{H}R_{1mn})\gamma_{1mn}{}^{V}_{H}\Phi_{1mn}(\rho, \varphi) \\
&+ {}^{V}_{H}R_{2mn}k\tilde{\varepsilon}{}^{V}_{H}\Phi_{2mn}(\rho, \varphi)] \quad (15)
\end{aligned}
$$

where ${}^{V}_{H}R_{jmn}$ and $\gamma_{jmn} = \sqrt{k^2 - g^2_{jmn}}$ are unknown amplitudes of the reflected TE ($j = 1$) and TM ($j = 2$) modes and their longitudinal propagation constants, ${}^{V}_{H}A_{1mn}$ are specified amplitude of the incident TE modes (excitation of the array by the TM modes is not of interest here) and $\tilde{\varepsilon} = 1$. The corresponding expressions for the transverse components of the field in the coaxial region of the aperture are obtained from (14) and (15) by substitution of ${}^{V}_{H}R_{2mn}$ and γ_{2mn} by unknown amplitudes ${}^{V}_{H}\hat{R}_{2mn}$ of the reflected TM modes and their propagation constants $\hat{\gamma}_{2mn} = \sqrt{k^2 - \hat{g}^2_{2mn}}$ in the layer, respectively, as well as $\tilde{\varepsilon}$ is substituted by ε.

The transverse components of the radiated electric and magnetic fields on the array aperture are represented as infinite sums of the vector Floquet harmonics

$$
\begin{aligned}
\boldsymbol{E}_{\tau}(x, y, +0) = &\sqrt{\mu_0/\varepsilon_0} \sum_{p,q} [T_{1pq}k\Psi_{1pq}(x, y) \\
&+ T_{2pq}\Gamma_{pq}\Psi_{2pq}(x, y)] \quad (16) \\
-\boldsymbol{e}_z \times \boldsymbol{H}(x, y, +0) = &\sum_{p,q} [T_{1pq}\Gamma_{pq}\Psi_{1pq}(x, y) \\
&+ T_{2pq}k\Psi_{2pq}(x, y)] \quad (17)
\end{aligned}
$$

where T_{jpq} are unknown amplitudes of the TE ($j = 1$) and TM ($j = 2$) modes, $\Gamma_{pq} = \sqrt{k^2 - w^2_{pq}}$, $w_{pq} = \sqrt{\alpha^2_p - \beta^2_{pq}}$, $\alpha_p = k \sin\theta \cos\varphi + 2\pi p/d_x$, and $\beta_{pq} = k \sin\theta \sin\varphi + 2\pi(q - p\Delta/d_x)/d_y$ are propagation constants, θ and φ are angles specifying the main beam direction, measured from the z and x axes, respectively, and

$$
\begin{aligned}
\Psi_{1pq}(x, y) &= \frac{1}{\sqrt{d_x d_y}} \frac{\boldsymbol{e}_x\beta_{pq} - \boldsymbol{e}_y\alpha_p}{w_{pq}} \exp[i(\alpha_p x + \beta_{pq} y)], \\
\Psi_{2pq}(x, y) &= \frac{1}{\sqrt{d_x d_y}} \frac{\boldsymbol{e}_x\alpha_p + \boldsymbol{e}_y\beta_{pq}}{w_{pq}} \exp[i(\alpha_p x + \beta_{pq} y)]
\end{aligned}
$$

are the orthonormalized vector wave functions of the TE and TM modes [5].

The projection matching of fields (14) and (15) and the corresponding representations for the layer region with fields (16) and (17) with account for the boundary condition on the flange

and orthogonality of the waveguide and Floquet modes on the corresponding regions leads to the system of linear algebraic equations

$$\begin{aligned}
&\gamma_{1m'n'}\,{}^{V}_{H}R_{1m'n'} + \sum_{p,q}\left({}^{V}_{H}S^{1m'n'}_{1pq}\Gamma_{pq}T_{1pq} + {}^{V}_{H}S^{1m'n'}_{2pq}kT_{2pq}\right)\\
&\quad = \gamma_{1m'n'}\,{}^{V}_{H}A_{1m'n'}\\
&\quad -{}^{V}_{H}R_{2m'n'} + \sum_{p,q}{}^{V}_{H}S^{2m'n'}_{2pq}T_{2pq} = 0\\
&\quad -\varepsilon\,{}^{V}_{H}\hat{R}_{2m'n'} + \sum_{p,q}{}^{V}_{H}\hat{S}^{2m'n'}_{2pq}T_{2pq} = 0\\
&-\sum_{m,n}{}^{V}_{H}S^{1mn*}_{1p'q'}\,{}^{V}_{H}R_{1mn} + T_{1p'q'} = \sum_{m,n}{}^{V}_{H}S^{1mn*}_{1p'q'}\,{}^{V}_{H}A_{1mn}\\
&\quad \sum_{m,n}\left(-k\,{}^{V}_{H}S^{1mn*}_{2p'q'}\,{}^{V}_{H}R_{1mn} + \gamma_{2mn}\,{}^{V}_{H}S^{2mn*}_{2p'q'}\,{}^{V}_{H}R_{2mn}\right.\\
&\qquad \left.+\hat{\gamma}_{2mn}\,{}^{V}_{H}\hat{S}^{2mn*}_{2p'q'}\,{}^{V}_{H}\hat{R}_{2mn}\right) + \Gamma_{p'q'}T_{2p'q'}\\
&\quad = \sum_{m,n}k\,{}^{V}_{H}S^{1mn*}_{2p'q'}\,{}^{V}_{H}A_{1mn} \qquad (18)
\end{aligned}$$

where the asterisks denote complex conjugations, and the matrix elements are determined by the formulas

$$\begin{aligned}
&{}^{V}_{H}S^{1mn}_{1pq} = \int_0^{2\pi}\int_0^{b}{}^{V}_{H}\Phi_{1mn}\cdot\Psi_{1pq}\rho\,d\rho\,d\varphi\\
&\qquad = \frac{s_m}{N_{1mn}}\left[\frac{f}{w^2-g_1^2}\right.\\
&\qquad\quad \left.-\frac{\hat{g}_1^2 bZ_{1m}(\hat{g}_1 b)J'_m(wb)+f}{w^2-\hat{g}_1^2}\right]\begin{bmatrix}\cos\\ \sin\end{bmatrix}m\varphi_{pq}\\
&f = g_1 a[wJ'_m(g_1a)J_m(wa) - g_1J_m(g_1a)J'_m(wa)]\\
&{}^{V}_{H}S^{1mn}_{2pq}\\
&\quad = \int_0^{2\pi}\int_0^{b}{}^{V}_{H}\Phi_{1mn}\cdot\Psi_{2pq}\rho\,d\rho\,d\varphi\\
&\quad = \mp\frac{s_m m}{N_{1mn}}\\
&\qquad\cdot\frac{[J_m(g_1a)-Z_{1m}(\hat{g}_1a)]J_m(wa)+Z_{1m}(\hat{g}_1b)J_m(wb)}{w}\\
&\qquad\cdot\begin{bmatrix}\sin\\ \cos\end{bmatrix}m\varphi_{pq}\\
&{}^{V}_{H}S^{2mn}_{2pq} = \int_0^{2\pi}\int_0^{a}{}^{V}_{H}\Phi_{2mn}\cdot\Psi_{2pq}\rho\,d\rho\,d\varphi\\
&\qquad = -s_m\frac{g_2aJ_m(g_2a)}{N_{2mn}}\frac{wJ_m(wa)}{w^2-g_2^2}\begin{bmatrix}\sin\\ \cos\end{bmatrix}m\varphi_{pq}\\
&{}^{V}_{H}\hat{S}^{2mn}_{2pq}\\
&\quad = \int_0^{2\pi}\int_a^{b}{}^{V}_{H}\hat{\Phi}_{2mn}\cdot\Psi_{2pq}\rho\,d\rho\,d\varphi\\
&\quad = s_m\frac{\hat{g}_2 w}{\hat{N}_{2mn}}\\
&\qquad\cdot\frac{aZ'_{2m}(\hat{g}_2a)J_m(wa)-bZ'_{2m}(\hat{g}_2b)J_m(wb)}{w^2-\hat{g}_2^2}\begin{bmatrix}\sin\\ \cos\end{bmatrix}m\varphi_{pq}
\end{aligned}$$

for $m\neq 0$ and $n\neq 1$ simultaneously and

$${}^{V}_{H}\hat{S}^{201}_{2pq} = i\sqrt{\frac{2\pi}{d_x\,d_y\,\ln(b/a)}}\,\frac{J_0(wa)-J_0(wb)}{w}$$

where $s_m = 2\pi i^{m+1}(d_x\,d_y)^{-1/2}$, $\varphi_{pq} = \operatorname{arctg}(\beta_{pq}/\alpha_p)$, and the subscripts pq at w_{pq} as well as those mn at g_{1mn}, g_{2mn}, $\hat{g}_{1mn}$, and $\hat{g}_{2mn}$ are omitted for brevity.

The amplitudes of the reflected waveguide modes and radiated Floquet modes are determined as a result of a numerical solution of the system (18), and are then used for calculation of the array element pattern, aperture efficiency, and other array characteristics.

III. Numerical Results and Discussion

A. Some Features of the TE Modes

The first stage in the solution of the problem formulated in Section II is a numerical analysis of the waveguide modes, which is based on solution of the corresponding dispersion equations. Note once more that unlike the indicated TM modes, the TE ones have not previously been studied in the literature, and their detailed analysis is a subject of a separate paper [10]. Since such an analysis is beyond the scope of the present study, we will only mention the most significant features of the TE modes.

The dispersion equation (10) is numerically solved with respect to $\hat{g}$. In principle, the circular waveguide with two-layer filling can support complex modes at some parameters of the filling. In our cases of small layer thickness and relatively small layer permittivity, the complex modes have not been detected and, therefore, the constant $\hat{g}$ is real and positive, while g determined by $\hat{g}$ from (4) can be either real or imaginary. In the latter case, the Bessel functions J_m of g should be correspondingly replaced by the modified Bessel functions I_m of $|g|$.

The first azimuth harmonic ($m = 1$) with the transverse propagation constant equal to zero corresponds to the hard wall condition. According to (11), the field in the central region of the waveguide is in this case a uniform linearly polarized plane wave and equation (10) can be rewritten in the form

$$J_1(k\tilde{a})N'_1(k\tilde{b}) - N_1(k\tilde{a})J'_1(k\tilde{b}) = 0 \qquad (19)$$

where $\tilde{a} = (\varepsilon-1)^{1/2}a$ and $\tilde{b} = (\varepsilon-1)^{1/2}b$. The numerical solution for the first root of (19) is presented in Fig. 2 as the normalized layer thickness $(\tilde{b}-\tilde{a})/\lambda$ versus the normalized inner radius $\tilde{a}/\lambda$. Such a form of representation is more universal than the curves given in [2] and allows us to determine the layer thickness corresponding to the hard wall for a wide range of ε and a.

The mode corresponding to the hard wall as indicated above is assumed to be the operating mode corresponding to the dominant TE_{11} mode of an empty waveguide. However, the root of (10) for this mode has the second ordinal number. Nevertheless, to keep the correspondence mentioned above, we design it as $\hat{g}_{111}$ while the first root designed as $\hat{g}_{110}$, ($\hat{g}_{110} < \hat{g}_{111}$), corresponds to the so-called stripline mode [11], [12]. The role of the latter, which is a surface wave having no cutoff, will be noted below.

Numerical solution of (10) as well as its approximate analytical solution for the cases when the order of the Bessel function is much grater than its argument show that the stripline modes exist not only for the first azimuthal harmonic but also for all higher order harmonics. For the axially symmetrical modes, i.e.,

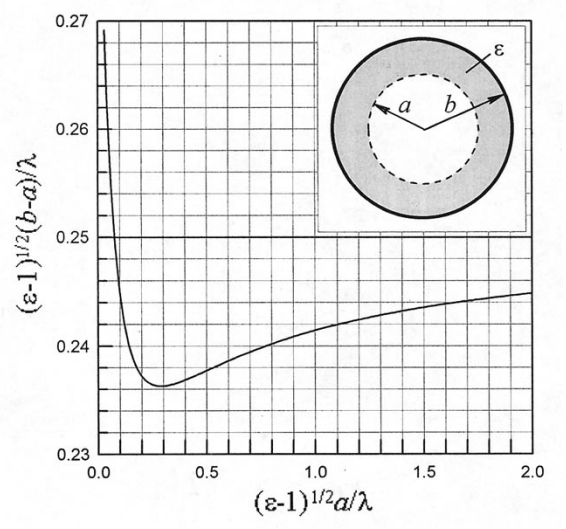

Fig. 2. Normalized layer thickness corresponding to the hard wall condition versus normalized inner radius.

$m = 0$, the magnetic field has no azimuthal component and, therefore, the longitudinal strips have no effect for this case.

Calculation of the propagation constants has been tested by comparison of the results with data available in the literature. For example, the calculated propagation constants of the operating mode TE_{11} and stripline mode TE_{10} for a waveguide with $a = \lambda$, $b - a = 0.22a$, and $\varepsilon = 2.5$ are $\gamma_{111} = 1.019k$ and $\gamma_{110} = 1.5768k$, which are in a good agreement with the plots presented in Figs. 11 and 12 in [3].

B. Array Characteristics

The results to be discussed below have been obtained for excitation of the array by the operating TE_{11} modes of vertical or/and horizontal polarizations. The infinite algebraic system (18) has been truncated so that only waveguide and Floquet modes satisfying the conditions $\mathrm{Im}\{\gamma_{jmn}\} \leq 2k$ and $w_{pq} \leq 10k$ has been kept. After solving the truncated system (18), the components of the array-element pattern corresponding to the unit power of the incident wave have been calculated by formulas

$$F_\theta(\theta, \varphi) = (k/\gamma_{111})^{1/2} |T_{200}(\theta, \varphi)| \cos\theta$$
$$F_\varphi(\theta, \varphi) = (k/\gamma_{111})^{1/2} |T_{100}(\theta, \varphi)| \cos\theta. \qquad (20)$$

The square of the appropriate component of (20) at $\theta = 0$ corresponds to the array aperture efficiency for the broadside. The cross-polarization level has been calculated by using the technique given in [13]. In our notations, the cross polarization levels are determined by formulas

$$L^V = 20 \lg \left[\frac{1}{2} \left| \frac{F_\theta^V(\theta, \pi/2)}{F_\theta^V(0, \pi/2)} - \frac{F_\varphi^V(\theta, 0)}{F_\varphi^V(0, 0)} \right| \right]$$
$$L^H = 20 \lg \left[\frac{1}{2} \left| \frac{F_\varphi^H(\theta, \pi/2)}{F_\varphi^H(0, \pi/2)} - \frac{F_\theta^H(\theta, 0)}{F_\theta^H(0, 0)} \right| \right] \qquad (21)$$

where superscripts V and H denote vertical and horizontal polarization of excitation. The calculations has been controlled by verification of the energy balance relationship as well as by other checks recommended in [5].

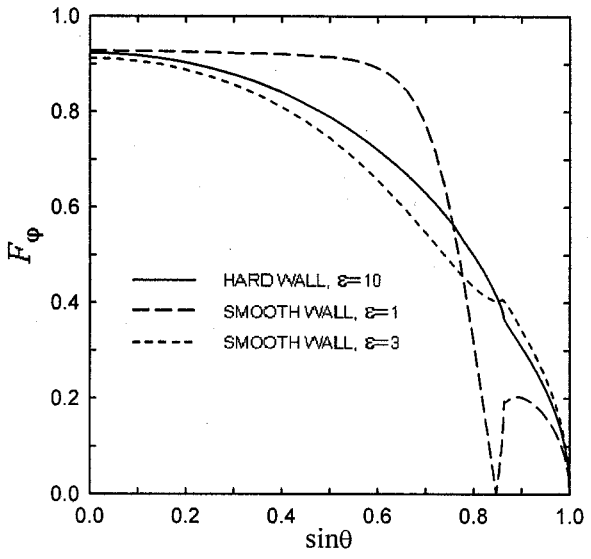

(a)

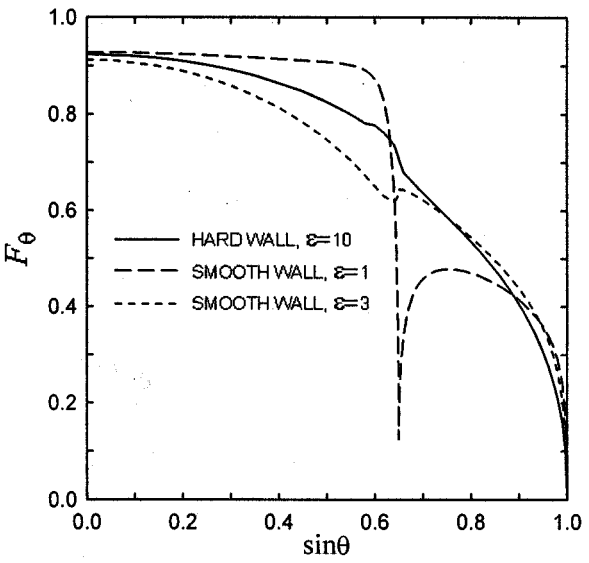

(b)

Fig. 3. Element patterns of waveguide array with $b = 0.32\lambda$, $d_x = 0.7\lambda$, $d_y = d_x\sqrt{3}/2$, and $\Delta = d_x/2$ (hexagonal lattice) at vertical polarization of excitation. (a) Horizontal plane. (b) Vertical plane.

The influence of the hard strip-loaded walls on the performance of arrays with relatively small-element spacing is illustrated by an array of waveguides of radius $b = 0.32\lambda$ arranged over a hexagonal lattice with $d_x = 0.7\lambda$. The hard wall condition is realized by strip-loaded dielectric layers with $\varepsilon = 10$ and $b - a = 0.08\lambda$. The waveguides are excited by the operating modes TE_{11} of vertical polarization. The array-element patterns in the horizontal (F_φ) and vertical (F_θ) planes are shown by solid curves in Fig. 3(a) and (b), respectively. The comparison is made with the case of smooth-walled empty waveguides excited by the dominant TE_{11} modes of vertical polarization. The element patterns for this case are shown in Fig. 3(a) and (b) by

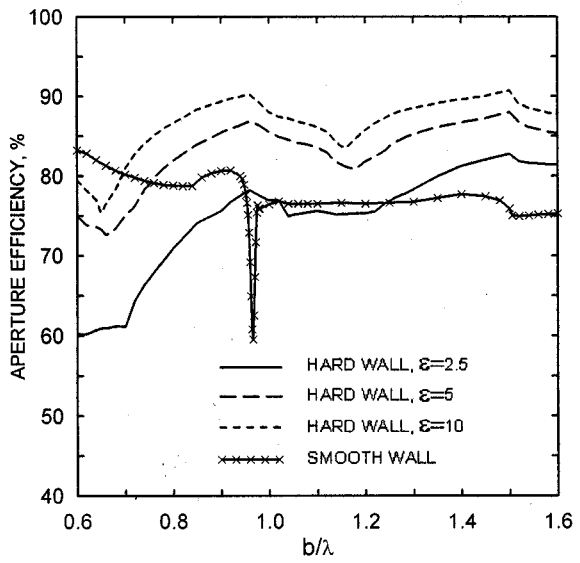

Fig. 4. Aperture efficiency versus radius of waveguide for array with $d_x = 2b + 0.05\lambda$ $d_y = d_x\sqrt{3}/2$, and $\Delta = d_x/2$ (hexagonal lattice).

the curves with large dashes. The patterns have dips causing the effects of blindness in both main planes for the indicated polarization [5]. We see that like in arrays of rectangular waveguides [14], the hard walls remove the dips. However, the element pattern tapers off faster corresponding to increasing the reflected power when deflecting the main beam from the broadside. The reflected power is mainly transferred by the propagating operating mode TE_{11}, strip-line mode TE_{10}, stripline modes of higher orders and coaxial TEM mode, although the latter is not excited when scanning in the H-plane. The hard wall waveguide, therefore, is multimode and its operation is similar to that of a smooth wall waveguide completely filled with an appropriate dielectric. This conclusion is illustrated by the element patterns shown in Fig. 3(a) and (b) with short dashes, corresponding to a dielectric with $\varepsilon = 3$ when the propagating modes are TE_{11}, TE_{21}, and TM_{01}. Note that the element patterns of the hard wall waveguide array for the horizontal polarization are similar to those of the vertical polarization, while the patterns of the empty smooth wall waveguides have no dips for the horizontal polarization [5], which significantly differ from the case of vertical polarization.

Thus, the example presented above as well as some similar results not included here confirm the conclusion made in [15] regarding partial filling of a waveguide cross section with dielectric. The indicated filling including the hard wall case does not give any significant advantages in comparison with a uniform filling from the viewpoint of achieving good of wide-angle scanning performance. However, the partial filling allows savings in dielectric material and decreases the weight, which is of interest for many applications.

The use of the strip-loaded dielectric hard walls gives significantly better results for waveguides of larger diameters. The aperture efficiency versus radius of an individual hard open-ended waveguide approximately calculated by the method of Huygen–Kirchoff without accounting for the reflections

TABLE I
PERCENT DISTRIBUTION OF REFLECTED POWER OVER MODES OF HARD WALL WAVEGUIDE

	$b = 0.9\lambda$			$b = 1.3\lambda$		
Modes	ε=2.5	ε=5	ε=10	ε=2.5	ε=5	ε=10
TE_{10}	1.90	2.19	1.42	0.84	0.92	0.69
TE_{11}	0.74	1.17	0.89	0.29	0.38	0.34
TE_{12}	1.33	1.24	1.18	0.23	0.28	0.28
TE_{13}	–	–	–	0.74	0.76	0.69
TM_{11}	4.30	2.71	1.90	0.51	0.56	0.43
TM_{12}	–	–	–	–	1.43	1.01
Others	0.53	0.09	0.21	0.09	0.07	0.16
Total	8.80	7.30	5.60	2.70	4.40	3.60

from the aperture has been presented in [2] for different values of the layer permittivity. The similar results, but for hard waveguides in an array, are presented in Fig. 4. The lattice of the array is hexagonal with spacing $d_x = 2b + 0.05\lambda$. Note that the presented aperture efficiency for the broadside is independent of polarization. This fact follows from the system (18) and is explained by the circular symmetry of the waveguide itself and by the symmetry of its excitation including the mutual coupling. We see that unlike the monotonically increasing functions in [2], the aperture efficiency of the hard waveguide in an array versus radius has an oscillatory shape. Such a behavior is explained by changing the number and position of the array factor grating lobes in free-space [16] as well as by changing the number of propagating modes in the waveguide. Another difference is due to the aperture efficiency itself. To avoid confusion, note that the aperture efficiency for an individual waveguide is determined with respect to its aperture area πb^2, while the efficiency of an element in an array is determined with respect to the area of the array cell $d_x\, d_y$. Therefore, the limit of the aperture efficiency when $b \to \infty$ amounts to 100% for an individual hard wall waveguide and to $(\pi b^2/d_x\, d_y) \times 100\%$ for the same waveguide in an array. The latter limit for the case of a fixed gap between the waveguides is equal to $0.5\pi/\sqrt{3} \approx 90.7\%$. Therefore, it is not possible to obtain 100% aperture efficiency in arrays of circular waveguides with large apertures.

Some results characterizing the contribution of certain waveguide modes into the reflected power for two values of the hard wall waveguide radius are presented in Table I. The total reflected power reduces when the waveguide radius and layer permittivity increase, as expected. The calculations show that the reflection of the operating mode TE_{11} itself is insignificant. The main contribution to the reflected power is made by the higher order modes. It should be noted in this connection that in a real horn fed through a single-mode waveguide, the higher order modes will be rereflected from the horn throat and returned back to the aperture, affecting thereby the horn performance, in particular, the aperture efficiency behavior discussed above. However, the study of such a situation is beyond the scope of this paper.

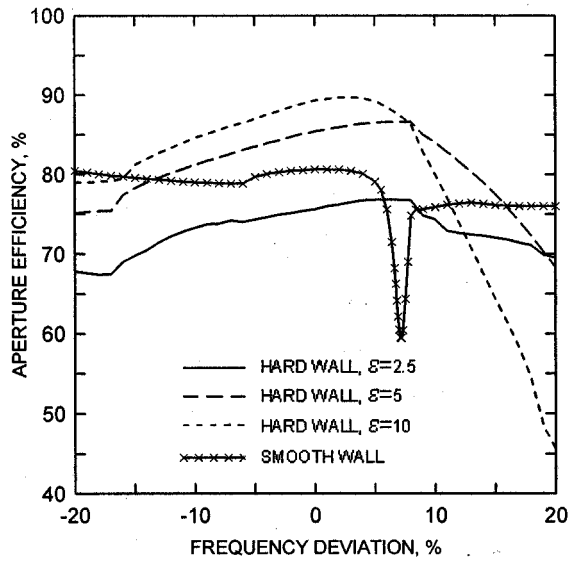

(a)

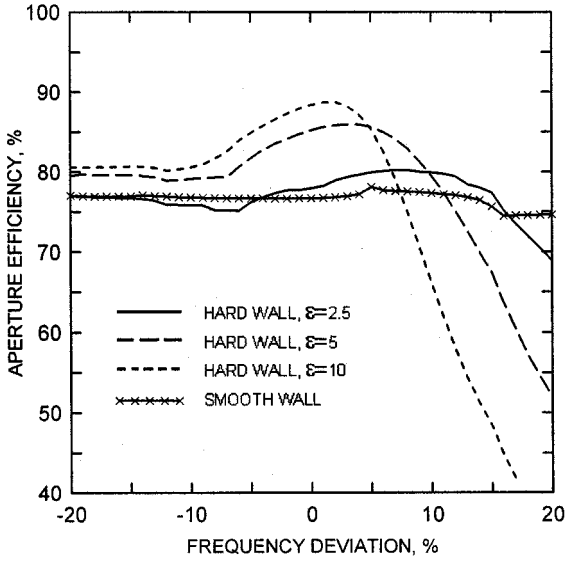

(b)

Fig. 5. Aperture efficiency versus frequency deviation for array with $d_x = 2b + 0.05\lambda$, $d_y = d_x\sqrt{3}/2$, and $\Delta = d_x/2$ (hexagonal lattice). (a) $b = 0.9\lambda$. (b) $b = 1.3\lambda$.

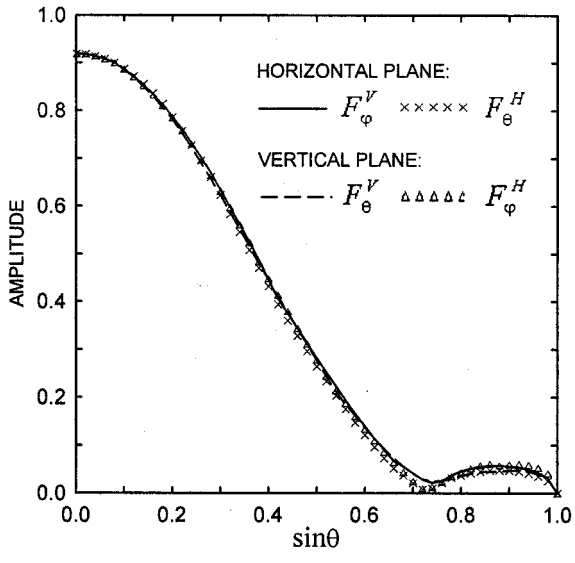

(a)

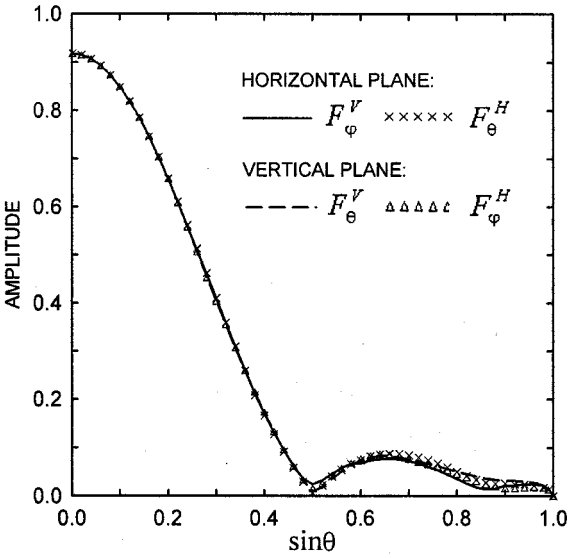

(b)

Fig. 6. Element patterns in main planes of array with $d_x = 2b + 0.05\lambda$, $d_y = d_x\sqrt{3}/2$, $\Delta = d_x/2$ (hexagonal lattice), and $\varepsilon = 5$ at vertical (V) and horizontal (H) polarization. (a) $a = 0.784\lambda$, $b = 0.9\lambda$. (b) $a = 1.181\lambda$, $b = 1.3\lambda$.

The solid curve with crosses shown in Fig. 4 for comparison corresponds to the aperture efficiency of an array of empty smooth wall waveguides. In the indicated range of the waveguide radius, such an array is characterized by low (less than 1%) level of reflected power except for the region near the anomaly (its nature is similar to that of the dips in the element patterns shown in Fig. 3 and in [5]) where the reflected power reaches nearly 14%, and the aperture efficiency respectively decreases down to 59%. The calculations show that if the layer permittivity is greater than 2.5, the hard walls provide higher aperture efficiency than for the smooth wall case when the waveguide radii exceed 1.25λ. If the layer permittivity is greater than five, the indicated advantage takes place even for $b > 0.75\lambda$. The hard waveguide in [2] was seen to have advantages compared to both soft and smooth waveguides. The present analysis shows that the advantages are not so significant. This discrepancy is explained by the loss in the hard waveguides caused by the interactions between the array elements and the power reflections that were not taken into account in [2].

The behavior of the hexagonal array aperture efficiency in a frequency band is illustrated by the examples given in Fig. 5(a) and (b) for the waveguide radius of 0.9λ and 1.3λ, where λ is the wavelength at the reference frequency. We see that the aperture efficiency for the hard waveguides is more frequency sensitive than the aperture efficiency for the smooth wall waveg-

uides, outside the anomaly region mentioned above. Such a behavior is similar to that for the case of a dielectrically loaded hard parallel-plate waveguide array [17] and is explained by the deformation of the shape of the operating mode field distribution over the waveguide cross section when the frequency changes. When the frequency increases from the reference value, the field concentrates more to the layer region that results in increased power reflected from the aperture and power scattered into the sidelobes. The aperture efficiency reduction when the frequency decreases is not so fast as when it increases, because the redistribution of the field from the layer region into the central region, which takes place in this case, only leads to broadening the main lobe of the element pattern without increasing the sidelobes and significant changing the reflected power.

In addition to the aperture efficiency, we have studied the cross-polarization level (21) over a frequency band. The results obtained for the array indicated in the previous example show that the cross-polarization level does not exceed -30 dB for levels above -12 dB in the main lobe of the element pattern for vertical and horizontal polarizations. The waveguides with $b = 0.9\lambda$ provide the band from -17% to $+3\%$ at $\varepsilon = 5$ and from -12% to $+2\%$ at $\varepsilon = 10$. The similar band for the waveguides with $b = 1.3\lambda$ is from -16% to $+2\%$ and from -8% to $+1.5\%$, respectively. The lowest level of the cross polarization for the array under consideration is achieved at the frequencies near 0.95 of the reference value, which is in agreement with the results of [2]. Similar effects can be obtained at the reference frequency but only if the layer thickness is correspondingly smaller than that of hard value. The examples of the element patterns calculated for the array with $a = 0.784\lambda$ and $a = 1.181\lambda$ at $\varepsilon = 5$, while the inner layer radii for the hard wall are $a \approx 0.7781\lambda$ and $a \approx 1.1772\lambda$, respectively, are shown in Fig. 6(a) and (b). The cross-polarization level (21) is, in this case, lower than -30 dB everywhere in space.

IV. Conclusion

In this paper, we have considered an infinite planar periodic antenna array of open-ended circular waveguides with hard walls formed on the basis of strip-loaded dielectric layers. The array has been analyzed by the mode-matching method. The waveguide modes involved in the method have been calculated by using the asymptotic strip boundary condition (ASBC). It is shown that the waveguide modes are divided into an independent subsystem of TE modes for the whole cross section and two independent subsystems of TM modes: one is for the central region and another is for the layer region. The high efficiency of applying the ASBC is confirmed once more by comparison of the results obtained in this study to those available in the literature.

The results for arrays of small waveguide diameters and spacing, which are usually chosen for providing wide-angle scanning have shown that the operation of the hard wall waveguides is similar to that of the smooth wall multimode waveguides completely filled with appropriate dielectric. However, the use of the hard waveguides allows savings in dielectric material and reducing the design weight that is of great importance for some applications.

The results obtained for arrays with elements of large diameters and spacing, at which the hard waveguides provide significant advantages over the smooth wall ones, have revealed the following features. First, it is shown that, unlike the case of an individual waveguide, the array aperture efficiency does not increase monotonically when the waveguide radius increases. Second, the advantages of the hard waveguides over the smooth ones are less significant than what follows from the results in [2], mainly due to power reflections from the waveguide aperture. It is shown that the main contribution to the reflected power is made by the modes TM_{11} and TM_{12} (if the latter is propagating) of the central waveguide region, as well as by the stripline mode TE_{10}.

The behavior of the aperture efficiency and the level of the cross polarization in a frequency band studied in the present work in general confirms the results and conclusions published in the literature before.

Acknowledgment

The authors would like to thank Dr. B. K. Gol'berg and Dr. Y. B. Korchemkin of Joint-Stock Company "Radiophyzika," Moscow, Russia, for useful discussions.

References

[1] P.-S. Kildal, "Definition of artificially soft and hard surfaces for electromagnetic waves,," *Electron. Lett.*, vol. 24, pp. 168–170, Feb. 1988.

[2] E. Lier, "Hard waveguide feeds with circular symmetry for aperture efficiency enhancement," *Electron. Lett.*, vol. 24, pp. 166–167, Feb. 1988.

[3] ——, "Analysis of soft and hard strip-loaded horns using a circular cylindrical model," *IEEE Trans. Antennas Propagat.*, vol. 38, pp. 783–793, June 1990.

[4] B. L. Diamond, "A generalized approach to the analysis of infinite planar array antennas," *Proc. IEEE*, vol. 56, pp. 1837–1851, Nov. 1968.

[5] N. Amitay, V. Galindo, and C. P. Wu, *Theory and Analysis of Phased Array Antennas*. New York: Wiley, 1972.

[6] P.-S. Kildal, A. Kishk, and Z. Sipus, "Asymptotic boundary conditions for strip-loaded and corrugated surfaces," *Microwave Optical Technol. Lett.*, vol. 14, pp. 99–101, Feb. 1997.

[7] A. A. Kishk and P.-S. Kildal, "Asymptotic boundary conditions for strip-loaded scatterers applied to circular dielectric cylinders under oblique incidence," *IEEE Trans. Antennas Propagat.*, vol. 45, pp. 51–56, Jan. 1997.

[8] Z. Sipus, R. Zentner, and J. Bartolic, "Validity of approximate boundary conditions for periodic strips on cylindrical surfaces," in *1998 Int. Conf. Math. Methods Electromagn. Theory (MMET'98)*, vol. 1, Kharkov, Ukraine, June 1998, pp. 171–173.

[9] L. A. Weinstein, *Electromagnetic Waves*. Moscow, Russia: Radio Svyaz' Press, 1988.

[10] S. P. Skobelev and P.-S. Kildal, "Eigen waves of a circular waveguide with a hard wall on the basis of a strip-loaded dielectric layer," Telecommun. Radio Eng., to be published.

[11] M. S. Aly and S. F. Mahmoud, "Propagation and radiation behavior of a longitudinally slotted horn with dielectric-filled slots," *Proc. Inst. Elect. Eng.*, pt. H, vol. 132, no. 7, Dec. 1985.

[12] Z. Sipus, H. Merkel, and P.-S. Kildal, "Green's functions for planar soft and hard surfaces derived by asymptotic boundary conditions," *Proc. Inst. Elect. Eng. Microwaves, Antennas, Propagat.*, vol. 144, pp. 321–328, Oct. 1997.

[13] T. Scharten, J. Nellen, and F. van den Bogaart, "Longitudinally slotted conical horn antenna with small flare angle," *Proc. Inst. Elect. Eng.*, pt. H, vol. 128, pp. 117–123, June 1981.

[14] S. P. Skobelev and P.-S. Kildal, "Blindness removal in arrays of rectangular wave-guides using dielectrically loaded hard walls," *IEEE Trans. Antennas Propagat.*, vol. 46, pp. 546–550, Apr. 1998.

[15] P. J. Wood and E. A. Pacello, "Phased-array antennas with dielectric fin aperture loading," *IEEE Trans. Antennas Propagat.*, vol. AP-23, pp. 824–829, Nov. 1975.

[16] G. T. Markov and D. M. Sazonov, *Antennas*. Moscow, Russia: Energiya, 1975.
[17] S. P. Skobelev, L. L. Mukhamedov, and P.-S. Kildal, "Effect of dielectrically loaded hard walls on performance of waveguide antenna arrays," *J. Int. de Nice Sur Les Antennes*, pp. 634–637, Nov. 1996.

Sergei P. Skobelev (M'96) was born in Kaluga Region, Russia, on September 25, 1953. He received the M.S. and Ph.D. degrees in antennas and microwave engineering from the Moscow Institute of Physics and Technology (MIPT), U.S.S.R., in 1977 and 1984, respectively.

From 1977 to 1981, he was a Research Engineer at the Research Institute of Radio Physics (now Joint-Stock Company (JSC) "Radiophyzika"). Since 1985, he has been with the Antenna Department of JSC "Radiophyzika" as a Leading Engineer (1985–1987), a Research Associate (1987–1991), a Senior Research Associate (1991–1998), and a Leading Research Associate (1998 to the present). He took part in a number of main Russian and international projects performed at JSC "Radiophyzika." He is the author and coauthor of more than 60 published works and reports, including 19 articles in international and Russian academic journals, 24 papers at Russian and international conferences, and seven Soviet Union author's certificates for inventions. His main area of scientific interests include the electrodynamics of periodic structures, array antenna theory and technology, as well as analytical and numerical methods in electromagnetics. He also gives lectures on applied electromagnetics for the students of MIPT and was a Scientific Advisor of a few students and Ph.D. students of MIPT.

Dr. Skobelev was one of the organizers of the International School-Seminar on Wave Diffraction and Propagation and two International Conferences on Antenna Theory and Technology, Moscow, in 1993, 1994, and 1997, respectively.

Per-Simon Kildal (M'82–SM'82–F'95) was born in Norway on July 4, 1951. He received the M.S.E.E., Ph.D., and Doctor Technicae degrees from the Norwegian Institute of Technology (NTH), Trondheim, Norway, in 1976, 1982, and 1990, respectively.

He was with ELAB (Electronics Research Laboratory) at NTH from 1979 to 1989 and as a Principal Research Scientist from 1986. He is now a Professor at the Department of Microwave Technology at Chalmers University of Technology, Gothenburg, Sweden. Since 1984, he has been a Consultant for Cornell University, Ithaca, NY, in connection with the upgrading of the radiotelescope in Arecibo, Puerto Rico. He is also consulting for others via Kildal Antenna Consulting AB, where he also develops and markets commercial software for synthesis and analysis of reflector antennas. He has given invited lectures in plenary sessions at four conferences. He is the principal author of more than 40 articles in international journals and more than 40 papers at international conferences. He has also coauthored more than 30 articles and conference papers. All papers are within the area of antenna theory and design. His specialty is reflector antennas. He has been largely involved in the electrical design of some large antennas. He is the inventor of three patents and has additional applications pending. He served as a Distinguished Lecturer of the IEEE Antennas and Propagation Society from 1991 to 1994.

Dr. Kildal was awarded by ELAB in 1984 for his work in connection with an industrial project, where the results of his reflector antenna research were applied. He received the R.W.P. King Award for Best Paper and the S.A. Schelkunoff Transactions Prize Paper Award for Best Paper in IEEE TRANSACTIONS ON ANTENNAS AND PROPOGATION in 1984 and 1990, respectively. He was an elected member of IEEE Antennas and Propagation Society AdCom for the period 1995–1997, and served as an Associate Editor of the IEEE TRANSACTIONS ON ANTENNAS AND PROPAGATION from June 1995 through July 1998.